CARBON 49 (2011) 3332–3339

available at www.sciencedirect.com

ScienceDirect

journal homepage: www.elsevier.com/locate/carbon

Ring-shaped field emission patterns from carbon nanotube films

Bojan Zajec [a,*], *Vincenc Nemanič* [a], *Marko Žumer* [a], *Eugene N. Bryan* [b], *Robert J. Nemanich* [c]

[a] *"Jožef Stefan" Institute, Jamova 39, 1000 Ljubljana, Slovenia*
[b] *Department of Materials Science and Engineering, North Carolina State University, Raleigh, NC 27695, USA*
[c] *Department of Physics, Arizona State University, Tempe, AZ 85287-1504, USA*

ARTICLE INFO

Article history:
Received 7 October 2010
Accepted 9 April 2011
Available online 15 April 2011

ABSTRACT

Highly symmetric ring-shaped field emission patterns were observed from broad-area flat cathodes prepared by growing a film of vertically aligned carbon nanotubes (CNTs) on TiN coated Si substrates. The images were obtained utilizing a luminescent screen of a specially designed triode cell composed of parallel electrodes. The emission rings sporadically appeared during voltage scans in which the emission patterns and cathode currents were recorded. The fine structure and stability of the rings suggests that their formation is due to an emission state of an individual CNT. The observed patterns are consistent with models that predict the formation of emission rings produced by the inhomogeneous electron emission from CNTs. The macroscopic value of the electric field when the rings were observed was between 0.7 and 2.5 V/μm, and the emission current corresponding to individual rings was estimated to be in the range of 2–4 μA. Numerical simulation of electron trajectories for sidewall emission from similar shaped metallic structures is in qualitative and quantitative agreement with the experimentally observed ring-shaped field emission patterns. The results also appear consistent with a recent model [Marchand M, Journet C, Adessi C, Purcell ST. Phys Rev B 2009;80:245425] based on thermal-field emission due to Joule heating.

1. Introduction

Shortly after the discovery of carbon nanotubes (CNTs) [1], significant attention was directed towards their potential application as field emission (FE) sources due to their unique physical, chemical and structural properties. CNTs exhibit substantial mechanical strength, chemical inertness and have high aspect ratios resulting in exceptional electric field enhancement effects which are favorable for field emission applications [2]. Considerable effort over the years has been devoted to the investigation and characterization of CNTs as field emitters for point-electron source applications such as electron microscopy [3]. When attempting to explain experimental observations using theoretical approaches, difficulties arise in efforts to model and understand the origin of field emitted electrons from these structures due to the variety of open-ended, close-ended, multi-walled or single-walled configurations that CNTs are found to exist in. Structured field emission patterns have been reported by various authors providing insight on the emission behavior from individual CNTs at the atomic level [4–6]. These patterns, typically symmetric, have been attributed to enhanced emission states and/or the atomic structure of the nanotube tip where conventional field emission theory predicts that the emission originates. Models

* Corresponding author: Fax: +386 1 4773440.
E-mail address: bojan.zajec@ijs.si (B. Zajec).
0008-6223/$ - see front matter
doi:10.1016/j.carbon.2011.04.020

have been developed to simulate the observed emission patterns from single CNTs by taking into consideration secondary interactions such as adsorbates or interference fringes [7–9]. Several reports [4,10–12], have specifically noted unique ring-shaped emission patterns commonly observed while CNT emitters are operated in the high current regimes. In some cases, discs were observed to possess a hollow center which was explained by emission from an open ended tube [13]. In addition, structured patterns were also observed within the ring-like patterns, and it was suggested that the emission originated from a closed nanotube tip [4].

The conditions for electron emission from an isolated CNT standing on a flat conductor are set primarily by the magnitude of the local electric field at its tip. For a perfect cylinder ending with a hemispherical cap, Laplace's equation for the electric field distribution can only be solved numerically. As a result, computational models were developed where length to diameter ratios are used as independent variables for several different tip structures. Resulting field enhancement factors can be determined for any particular case [14]. The work function of the emitter and anode-to-cathode spacing are additional critical parameters required to perform numerical simulations of the current distribution found at a flat anode. The common approach is to assume that electrons are available over the entire cap area, and the magnitude of the local electric field determines the tunneling probability. The electron trajectories are then calculated using the electric field where repulsive Coulomb forces among the emitted electrons are often taken into account [15,16].

Another theoretical analysis of emission from single-wall CNTs (SWCNTs) having 1 nm, 2 nm and 3 nm diameters predicts that single and multiple rings (concentric zones with various brightness) can be formed at the anode as a result of the non-uniform probability density of electron localization at the hemispherical cap caused by "quantum constraints imposed by specific spatial confinement" [17]. This model also predicts a situation where there is little emission current attributed to electrons extracted from the apex of a tip. This specific effect is only applicable in extremely high current conditions which could be far greater than the current carrying capabilities of a small diameter SWCNT.

A recent modeling study by Marchand et al. [18] has postulated that ring shaped emission patterns may originate from thermal-field emission due to Joule heating of the nanotubes. The model results indicate that at high temperatures, electrons emitted from the shank of the nanotube, but near the tip, are focused into a ring pattern. The study notes that for other materials thermal runaway is expected to occur, but the stable high temperature state may be unique to carbon nanotubes.

In this paper we report on the observation of highly symmetric ring-shaped field emission patterns, review corresponding models that predict this unique emission behavior and present our own simulation of FE patterns from CNTs.

2. Experimental

The flat broad-area field emission cathodes (FBAFECs) investigated here were prepared at North Carolina State University (NCSU) using a 1.5 kW ASTeX microwave plasma chemical vapor deposition (CVD) system equipped with an inductively heated stage. The CNT films were grown on TiN coated *n*-type Si substrates using a 20 nm thick Fe catalyst layer. The 25 nm thick TiN films were deposited using plasma-assisted reactive evaporation, and the Fe catalyst was deposited using electron beam evaporation. Prior to TiN deposition, the Si substrates were treated in a 10:1 HF dip to remove the native oxide from the surfaces. After catalyst deposition the substrates were loaded into the CVD reactor.

The CNT films were grown using acetylene (25 sccm) and ammonia (55 sccm) precursors. The growth was carried out at a pressure of 37 mbar, microwave power of 900 Watts and a substrate temperature of ~900 °C. Typical growth times ranged from 5 to 30 min. Prior to plasma initiation and CNT growth, the Fe containing substrates were pretreated in an ammonia/acetylene atmosphere at a temperature of ~650 °C for 2 min.

Field emission characterization of the FBAFECs was performed in two labs. A preliminary inspection was completed soon after films were grown in a diode cell with phosphor imaging screen at NCSU. Selected samples were further investigated in a triode imaging cell consisting of parallel electrodes and a phosphor imaging screen at the "Jožef Stefan" Institute. The advantage of the triode configuration compared to a standard diode cell is the large drift space between the grid and imaging screen (both were set to the same potential) which enables achievement of higher magnification images of the emitted electron distribution. The triode cell was designed to hold a 25.5 mm diameter FBAFEC with an active diameter of 20 mm ($A \sim 3\ cm^2$). The cell was composed of a 20 mm diameter fine metal grid and a 25 mm diameter luminescent screen fabricated on ITO coated glass using an ultrafine P-43 phosphor powder. The inter-electrode distances and grid parameters are given in Fig. 1. The cell was mounted in a glass envelope with electrical feed-throughs to provide electrical contact to the individually isolated emitter, grid, and luminescent screen. The electrical and physical separation between these electrodes was achieved by using brazed ceramic rings. The instruments were interfaced with a computer for automated voltage sourcing and data collection, and all

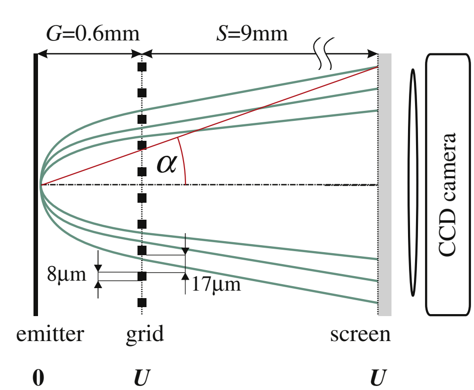

Fig. 1 – A schematic view of the imaging cell for observing 25.5 mm diameter FBAFECs with a 20 mm active diameter ($A \sim 3\ cm^2$). The semi-angle α between the ring center and its edge is marked.

measurements were obtained at pressures on the order of 1×10^{-8} mbar. Images of the luminescent screen were recorded using a CCD camera (DFK31F03) with a 1024×768 pixel resolution. The brightness of the luminescent screen was maintained well below saturation limits, and the exposure time of the CCD camera was adjusted to avoid over-exposure during the image capturing process.

A control experiment was developed using the same triode setup. A tungsten tip prepared by standard electrochemical etching methods (with a radius of curvature of ~25 nm) was mounted into the center of a 25 mm diameter stainless steel disk. It was estimated that the tip protruded ~1 mm from the base, while the estimated gap between the disk and the grid was ~2 mm and the screen-grid distance was ~9 mm. The images on the screen were analyzed in the same way as the measurements of the emission patterns observed on the FBAFEC.

3. Model adapted to particular electrode configuration

The focus of this study is to relate the ring patterns that are observed on the anode to the properties of the specific emission sites. For the purpose of modeling the trajectories of emitted electrons, it is not necessary to incorporate the specific emission mechanism as long as the initial velocity is negligible compared to final velocity. Hence, the electrons could be emitted through quantum mechanical tunneling as described by the Fowler–Nordheim expression, or due to thermal-field emission. After the emission the electrons will be accelerated through the field up to the grid. Beyond the grid the electrons will drift in a straight line.

We assume a classical description where the boundary conditions are linearly dependent on the applied voltage, so the magnitude of the electric field at any point is thus also linearly dependent on the applied grid potential. With this assumption, the path of an emitted electron (initially at rest) will be independent of the applied voltage. In our experiment this means that the projection of the image on the grid and on the screen should be independent of the applied voltage and macroscopic electric field.

In the following, a cylindrical coordinate system is used where the single emitter in the form of capped nanotube is parallel to the z-axis and grown from the origin. Assuming the emitter can be described as metallic, the local field at the point of emission is perpendicular to the surface, and the interaction with this field would provide the initial direction of the electron velocity. The local electric field far away from the CNT is almost identical to the uniform electric field of the parallel-plate capacitor (formed by the grid and substrate). As a reasoned starting point, we further assume that the electrons responsible for the ring formation have an initial velocity vector oriented predominantly in the lateral direction. This implies sidewall electron emission.

With these simplifications, the electrons beyond the CNT can be treated as emitted with an initial transverse velocity followed by a longer interaction with the average field which is normal to the substrate or grid surface. The electron trajectory could then be approximated as a parabolic path in the space up to the grid [19]. When the emitter length (l) is much less that the grid distance (G) or $l \ll G$, the radial coordinate r_g of the electron while passing through the grid plane can be related to G as

$$r_g = C\sqrt{G}, \qquad (1)$$

where C is a parameter having the dimension $m^{0.5}$. Its value is related to the transverse velocity which is dependent on the shape and dimensions of the emitting CNT. Since the grid and screen are at the same potential, the electron trajectories in this drift region are also independent of the applied voltage U. The parameter C contains the intrinsic properties of the emission that determines the electron beam spreading, irrespective of experimental conditions (G, U). The main observable quantity for each ring pattern is the radius r_s on the screen that is at distance S from the grid. Extrapolation of the tangent to the parabola $z = r^2/C^2$ at the grid plane provides the following relation:

$$r_s = \frac{C(2G+S)}{2\sqrt{G}}. \qquad (2)$$

Using this relation parameter C can be determined from the experimentally obtained r_s. In addition, its corresponding r_g can be determined from Eq. (1).

4. Results

A cross sectional SEM image of a CNT film grown on a TiN coated Si substrate is shown in Fig. 2(a), while a TEM image of a randomly selected CNT end is shown in Fig. 2(b). The film was grown for a total of 10 min and an approximate growth rate of 5 μm/min was determined. The nanotubes are vertically aligned with an average length of between 50 and 100 μm. Prior TEM studies of similar films have indicated that the CNTs have a 'bamboo' type internal structure and are multi-walled with approximately 5–10 concentric layers and diameters of between 50 and 100 nm.

After loading the FBAFEC samples into the triode cell, current vs. voltage (I–U) plots were generated by ramping the voltage in 25 V steps, Fig. 3. A dwell period of 35 s was used at each voltage increment, and the data was reproducible for consecutive forward sweeps. A threshold current was set to prevent overheating of the grid in the triode cell, and thus the maximum current recorded in the I–U plots does not represent the true limit of the FBAFEC.

Emission images were simultaneously recorded during the forward I–U sweeps of the FBAFEC samples. At any particular setting, the emission current was found to be relatively stable although a few fluctuations related to the turning on and off of individual emitters were observed on the imaging screen of the triode cell. At the higher current levels, emission rings were noted to occasionally appear. At voltages above the threshold of the luminescent screen, various patterns were observed with a majority of them showing irregular globular patterns. The rings were in general brighter and their diameters were larger than the globular patterns belonging to other individual emission sites. The ring patterns were also observed in the diode cell arrangement at NCSU, but their details were not displayed as clearly as in the triode cell. Examples of emission rings observed in the triode cell are

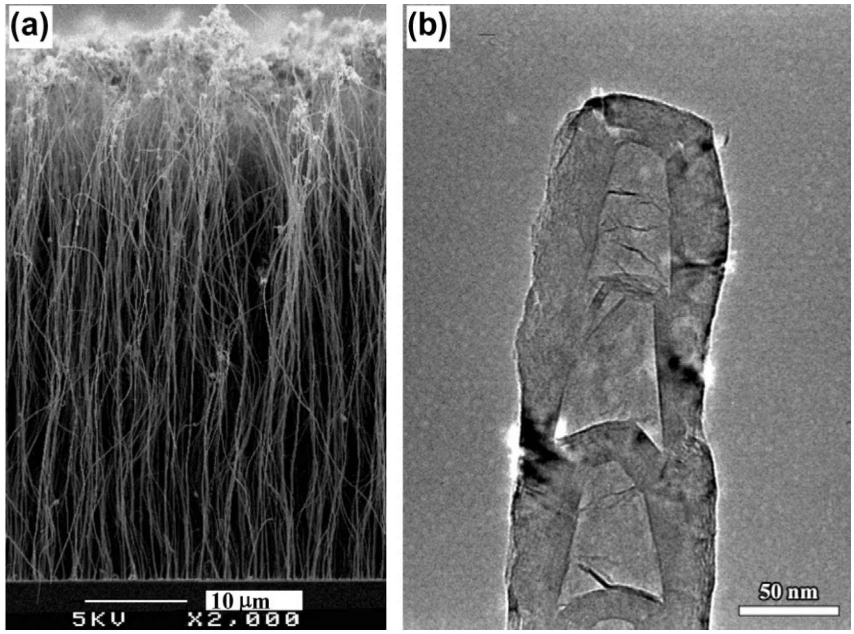

Fig. 2 – (a) A cross-sectional SEM image of a CNT film grown on a TiN coated Si substrate. The film was grown for a total of 10 min resulting in an approximate growth rate of 5 µm/min. (b) TEM image of a randomly selected CNT ending.

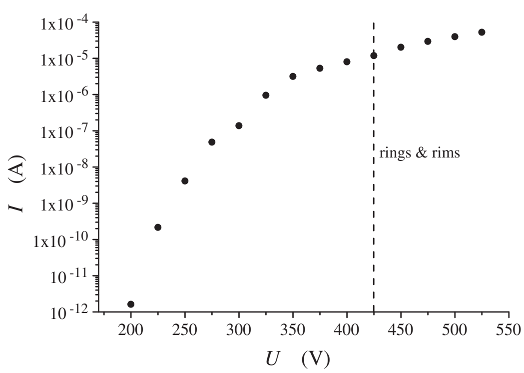

Fig. 3 – Typical *I–U* curve; a total current $I \sim 20\ \mu A$ was typically required for appearance of at least one ring/rim.

presented in Fig. 4. The rings were observed to abruptly appear at the various 25 V steps and were for the most part stable only over a small voltage range. Consequently, the emission rings would often disappear after an additional 25 V increase in voltage. The rings could often be reproduced by lowering the applied voltage.

On most CCD images, the contrast was sufficient to distinguish the shadow of the grid in bright regions of the image. The grid shadow superimposed on the CCD image of the entire luminescent screen represents only certain small areas of the entire grid and not the entire grid. The projection of the entire grid would require almost no magnification, meanwhile the grid spacing of 25 µm is magnified to ≈0.2 mm on the screen.

The fraction of the total current corresponding to a particular ring could not be measured directly in our experimental setup. We therefore made an indirect determination of the emission current related to an individual ring using the CCD image of the luminescent screen. The field emission current to a given spot on the luminescent screen is linearly proportional to the intensity of light emitted from this spot. In other words, pixel values in an image taken by a CCD camera are linearly correlated to the number of photons striking the corresponding elements in a CCD array. The spatial distribution of field emission current over the luminescent screen is thus linearly mapped in pixels of the digital image. This is only valid when the luminescent material and the CCD array are not saturated. The output of our CCD camera is a 24 bit RGB color image. The green layer in the CCD image was chosen to best represent the emission characteristics of the FBAFECs since the luminescent screen emits mostly in the green. The red and blue pixels were therefore discarded in the analysis, which gave pixel values within the range of 0–255 (8 bit). The component of the current corresponding to an individual ring could therefore be calculated from the sum of the pixel values.

In all of the recorded rings, background intensities existed due to additional emission sites that contributed to the excitation of the luminescent screen. The ring brightness was found to be at least 30–50% above the background level arising from other emission sites. The width of the concentric zone representing rings may be expressed in angular units. Most of them were narrow, 1–2° (FWHM), but a few were wider, up to several degrees. Due to the background intensity in the images of the emission rings, the brightness profile of the intensity distribution across the ring could not be determined accurately. However, it should be noted that in all cases, the ring brightness was higher than its central zone. In one particular image of a ring, the background intensity was low enough to allow a characteristic brightness profile line scan to be generated, Fig. 5. It is evident that the brightness of the ring is approximately five times higher than its

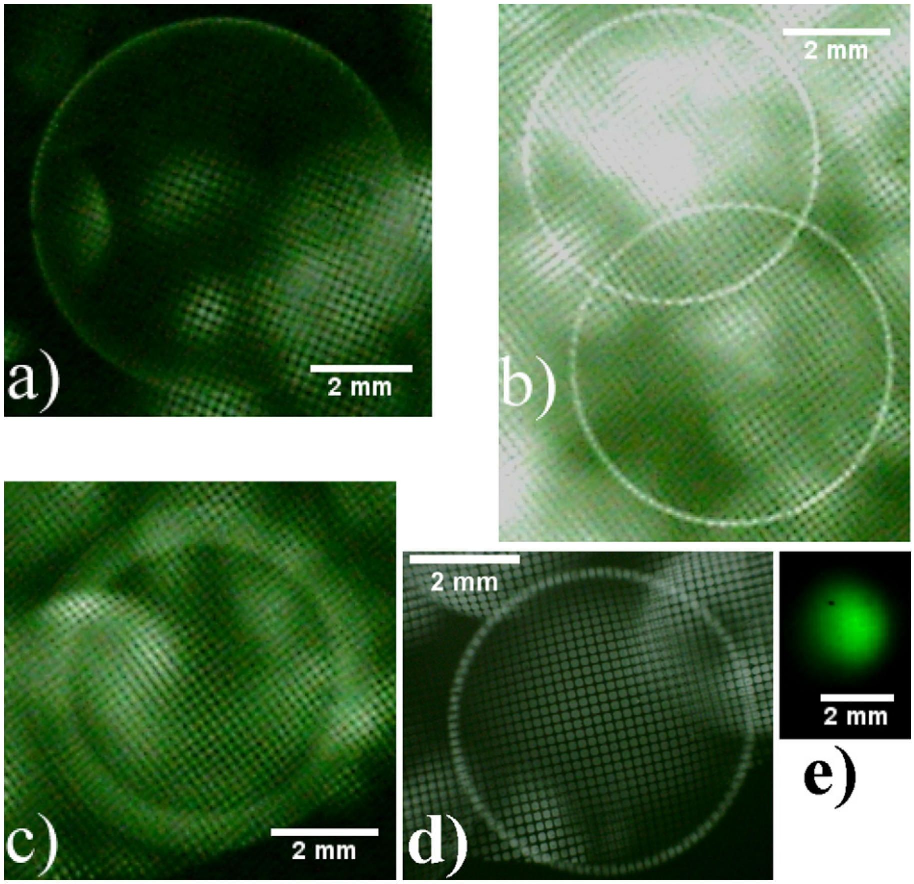

Fig. 4 – (a–d) Appearance of selected rings on the luminescent screen, (e) emission pattern from the etched W tip that was used as a control. Image (d) is also available as a high resolution image in the Supplementary Data section.

central zone. After examining temporal and voltage image sequences, it appeared that the diffuse pattern inside the ring was most likely due to electrons from other emitting sites.

Data collected on nine selected rings observed from various FBAFEC samples are listed in Table 1. The data given in the table are: ring radius r_s on the screen, the semi-angle α formed between the normal and the outer edge of the ring as displayed on the screen (Fig. 1), the macroscopic electric field E_m at which the ring appeared and the corresponding parameter C obtained from Eqs. (1) and (2).

To provide a control for these observations we measured the FE pattern from the etched W tip. The observed FE pattern is similar to a disc with the center as the brightest zone, Fig. 4(e). The FWHM semi-angle is 4.4° which is significantly smaller than values listed in Table 1. The extracting macroscopic electric field was 0.32 V/μm. If the sidewall emission model is assumed, the disc radius at the grid plane can be calculated which gives parameter C a value of 5.0 $\mu m^{0.5}$.

5. Discussion

The emission characteristics presented here are consistent with aspects of prior reports. The estimated average current density is on the order of a few mA/cm^2 at a macroscopic electric field of E_m = 0.5–2.5 V/μm. This is comparable to reported data for well-prepared FBAFECs with in situ grown or indirectly deposited CNTs [20]. The SEM image in Fig. 2(a) reveals that the CNTs are oriented predominantly perpendicularly to the surface. Prior TEM studies of similar films have indicated 5–10 concentric walls with a 'bamboo-like' inner structure. The caps of the CNTs appear to be closed and also multi-walled. SEM images of the surface typically show a low density of long CNTs that protrude from the surface at a large range of angles. It is most plausible that the observed emission is related to these protruding, longer CNTs, as it will be explained below. Most emission sites observed on the screen displayed a globular pattern which is attributed to emission from the closed tips of the CNTs. However, at this time we do not have the capability to correlate or identify a particular microscopic emission site with the pattern that appears on the screen.

Let us first comment on the narrow voltage ranges for the observation of individual ring patterns. The rings were predominantly observed to appear and disappear within single voltage steps of 25 V during the I–U sweeps, and they could often be observed multiple times during repeated increasing and decreasing I–U sweeps. Two possibilities to explain this effect may be considered: (1) rapid turn-on and then destruction due to heating, or (2) screening effects due to the presence of a few longer nearby nanotubes that become fully extended by the applied electric field. The fact that rings were observed during repeated voltage scans suggests that the

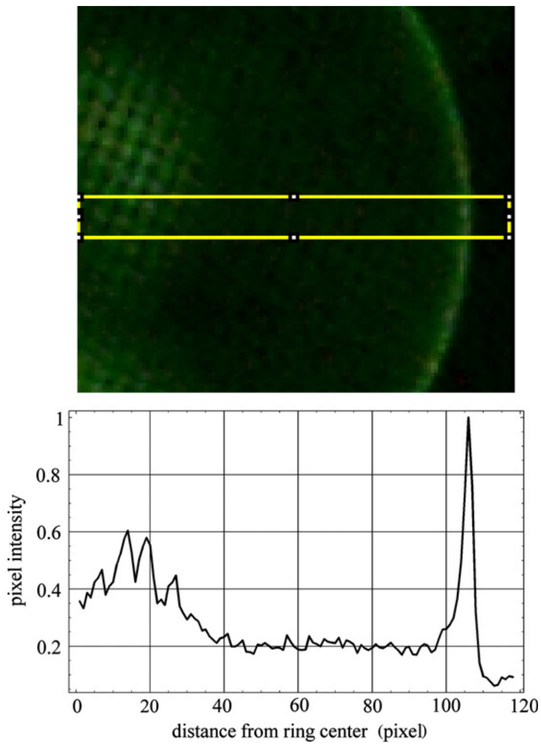

Fig. 5 – Section of ring No. 1 from Table 1 as seen on the luminescent screen. The brightness in the rectangle is vertically averaged and displayed below as the brightness profile. The cross-hatched modulation of the image is attributed to shadowing from the grid. The central diffuse region shows a different shadow pattern than the ring, which suggests that it originates from a different emitting site.

screening effect is the most likely explanation. Note that we have argued that the emission originates from the few nanotubes that extend substantially above the 'forest'. Thus, as the longest tubes are stretched vertically by the applied field, they may screen nearby emitting tubes. The screening process of nearby CNTs has been widely recognized as affecting the overall emission current from FBAFECs [21].

We turn now to consider the circular shape of the ring-shaped images. For a hemispherically capped metallic tube, the electron emission occurs predominantly from the cap apex where the electric field is the greatest. We have carried out a simulation of the electron trajectories for emission from metallic structures with dimensions similar to the nanotubes studied here in the same configuration as given in Fig. 1. Calculations of the electric field based on the classical Maxwell electrostatics and electron trajectories were completed using the Comsol Multiphysics program [22]. Initially we simulated the emission from a CNT ending with a hemispherical cap, where the tunneling probability from the cap was related to the local electric field by the simple Fowler–Nordheim [12] equation. The obtained emission pattern is disc-like with a maximum in the center. When the CNT is open-ended, or closed and flat-ended with the outer edge slightly rounded, the maximum electric field occurs at the rounded edge and has an initial emission direction approximately 45° away from the z-axis. Our simple simulation demonstrates that for particular CNT tip structures the appearance of ring patterns at the cathode is possible. However, the electrons emitted from such a rounded edge at ≈45° would yield a maximum radius $r_g = 225\ \mu m$ at a CNT length of 180 μm. On the other hand, the values of r_g evaluated from our observed r_s using Eqs. (1) and (2) are considerably larger, in the range of 270–430 μm. This discrepancy, along with the observed jagged cap surface, Fig. 2(b), which would not result in symmetric (ring-like) patterns, led us to reject the above model as an explanation for the ring formation. Further simulations revealed that an electron emission angle of almost 90°, i.e., side-wall emission, is required to obtain the observed radii. This requirement is in apparent contradiction with the location of the greatest electric field on any closed cap structure considered.

As noted in the introduction, a recent report by Marchand et al. [18] has suggested that the ring-shaped emission patterns could originate from thermal-field emission from capped nanotubes. According to their modeling results, at temperatures above 1800 K the emission pattern changes from a circular pattern with intensity maximum at the center to a pattern with an intense sharp ring. The main reasons for

Table 1 – Characteristics of nine selected ring-shaped emission patterns together with three patterns deduced from other reports. Notes: (a) smallest ring from a SWCNT [20], (b) largest ring from a SWCNT [20], (c) rings from SWCNTs [10].

	Radius on the screen r_s (mm)	Semi-angle α (deg)	Macroscopic electric field E_m (V/μm)	Beam spreading intensity C ($\mu m^{0.5}$)
1	3.6	20.8	0.83	17.5
2	3.2	18.2	0.71	15.2
3	3.0	17.2	0.75	14.3
4	2.8	16.5	0.88	13.7
5	2.7	15.8	0.75	13.1
6	2.6	14.9	0.71	12.3
7	2.3	13.7	0.75	11.3
8	2.3	13.3	0.88	10.9
9	1.6	9.4	2.50	7.7
10[a]	0.047	5.4	1.40	2.1
11[b]	0.14	15.9	1.40	6.4
12[c]	0.080	21.8	4.0	5.7

such behavior are different emission regimes at the CNT cap (thermally assisted Fowler–Nordheim) and CNT shank (Richardson/extended Schottky) [18]. The dependence on the temperature and local electric field is different for each of these two regimes. Consequently, at a sufficiently high temperature the emission from the CNT shank overwhelms the emission from the cap and leads to ring formation. The authors argue that the emission from the tip could be further suppressed due to the Nottingham cooling of the tip and reduction of the available electron population due to the emission from the shank. The voltage-dependent appearance of the rings could be attributed to the increased emission current from a CNT which would lead to an increase in its temperature. At a certain voltage, the local electric field and the increased temperature would combine to give rise to ring formation.

We simulated electron trajectories for sidewall emission from a single hemispherically capped tube with a diameter of 100 nm and a cylinder length of 70 μm, presented in Fig. 6. Initial electron positions were from 100 nm to 900 nm (in increments of 100 nm) below the cap-cylinder junction. Electrons are assumed to have zero initial kinetic energy. Evidently, the emission is transverse to the tube and a significant

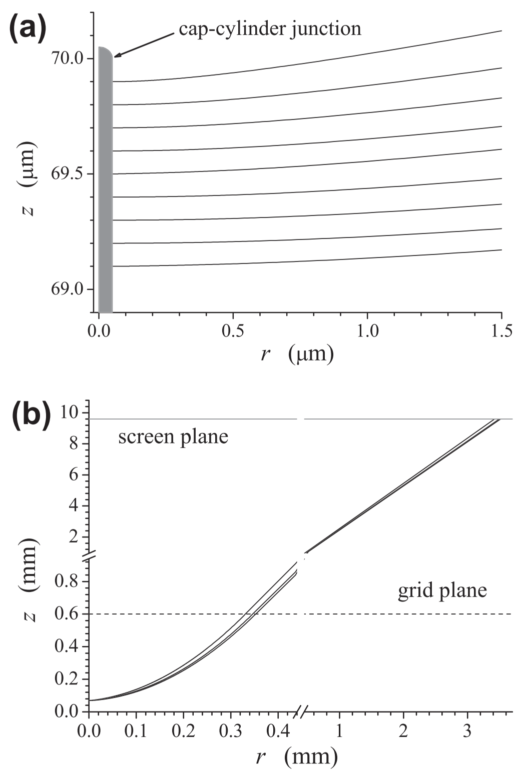

Fig. 6 – Calculated electron trajectories for sidewall emission from a spherical capped metallic tube with a 100 nm diameter and 70 μm cylinder length in an experimental setup as described in Fig. 1. Diagram (a) displays trajectories near the CNT surface, where initial electron positions are 100 nm, 200 nm, 300 nm, . . ., 900 nm below the cap-cylinder junction. Diagram (b) shows the nearly parabolic trajectories for the region below the grid plane and straight trajectories above the grid plane. The scale on both axes is broken to adequately visualize trajectories between the cathode and grid.

transverse velocity is acquired as the electron follows the trajectory away from the sidewall. At larger distances, the field is essentially the average field of the structure with a direction normal to the base plate. The nearly parabolic trajectories were evident for electron emission from the sidewall. Moreover, the electron trajectories remain bunched at the grid and continue to the screen which would result in a thin ring structure. Interestingly, a broadly similar experimental ion emission/ion optical effect, with a roughly similar proposed explanation, has been reported by Forbes [23]. In his report the emission from the shank of a field ion (FI) emitter was confirmed using a specimen with a specially prepared shape and hydrogen imaging gas.

Further analysis of the trajectories from this simulated nanotube structure yields an average $r_s = 3.47$ mm, $r_g = 340$ μm, and half angle of $\alpha = 19.8°$. Using these simulated values, the parameter C can be calculated from either Eq. (1) or Eq. (2). In the first case one obtains 14.4 $\mu m^{0.5}$ and in the latter 16.9 $\mu m^{0.5}$. The major reasons for the difference lie in the non-negligible length of the CNT tube and the parabolic approximation of the path.

The simulated case gives values very close to the average values obtained from the images studied here and listed in Table 1. Thus, it appears that sidewall emission accounts for the shape of the rings and the magnitude of the diameter.

Literature review revealed two publications [10,20] where actual dimensions of the observed ring-shaped emission patterns can be extracted. Their characteristics are added at the end of Table 1 for comparison. In both cases the experiment was done in the diode configuration, without the grid electrode. Assuming that sidewall emission (Eq. (1)) is valid for all rings in Table 1, the ring radius at the screen and semi-angle α are also dependent on the experimental setup dimensions G and S. As such, they are not suitable quantities for comparison between rings obtained in different experimental setups. Only the parameter C is device independent and it seems that the largest rings from [10,20] are comparable to our smallest rings. Thus, the macroscopic electric field does not seem to be correlated with the parameter C as predicted in section 3. This was also experimentally confirmed as the r_s remained constant for those few rings that were visible within several consecutive 25 V voltage steps.

In order to verify whether our CNTs reached sufficient temperatures to satisfy the explanation given in Ref. [18], the temperature of a typical observed CNT (70 μm length, 100 nm diameter) was calculated for field emission current equal to 4 μA. We applied a simple model including Nottingham cooling from Ref. [24] together with the data for electrical and thermal conductivities. As a boundary condition of the model, the substrate was held at a constant temperature equal to 300 K. The obtained temperature profile was significantly too low to account for the observations; primarily due to the large radius that reduces resistive heating and increases the radiation losses. When the diameter is reduced to 30 nm, the same simulation gives a temperature profile above 2200 K (maximum 2400 K) and a slightly higher temperature profile is obtained for an identical thin CNT with the length increased to 100 μm. Evidently, CNTs with a diameter of 30 nm or less and extending above the "forest" could emit ring-shaped patterns.

Although no such thin CNTs have been observed in investigated SEM images, this does not imply that they could not exist. Area density of such thin CNTs is extremely low since only a few rings have been observed from the entire cathode. Probability to find a single such CNT in SEM images that display only a small section of the entire cathode is therefore extremely low. It should be also noted that the diameter of the observed CNTs was in the range 50–100 nm. While the preceding analysis indicates narrower tubes than identified in our microscopy investigation it also seems to support the possibility that moderate changes in the modeling assumptions and/or emission from the thinnest extended tubes of the sample could account for the results presented here.

6. Summary

Ring-shaped field emission patterns were observed on the screen of a triode cell during routine *I–U* measurements of FBAFEC characteristics based on a PECVD film of multi-walled CNT. The projected sizes of the rings were large enough to allow detailed analysis. The rings were relatively stable patterns observed at constant voltage typically in the range of ~500 V just after a 25 V step in the applied voltage. The ring images often disappeared after the next 25 V step. The emission current that corresponded to one of the rings was estimated to be ~2–4 μA. The reproducible voltage-dependent appearance of the ring-shaped pattern was proposed to be ascribed to emission from a few long nanotubes that become fully extended by the applied electric field, and the voltage-dependent CNT temperature increase which could lead to conditions for predominant emission from the CNT shank [18]. The disappearance of the ring-shaped pattern during voltage increasing might be attributed to the screening of a few longer nearby nanotubes that become fully extended by the increased applied electric field. It was shown by simulation, that the large rings can be described only by emission from the sides of the nanotubes. While the emission patterns could not be described by typical emitter shapes, the results do appear to be consistent with a recently proposed model based on Joule heating and thermal-field emission [18].

Acknowledgement

This work was supported by the Slovenian Research Agency.

Appendix A. Supplementary data

Supplementary data associated with this article can be found, in the online version, at doi:10.1016/j.carbon.2011.04.020.

REFERENCES

[1] Iijima S. Helical microtubules of graphitic carbon. Nature (London) 1991;354:56–8.
[2] Coll BF, Dean KA, Howard E, Johnson SV, Johnson MR, Jaskie JE. Nano-emissive display technology for large-area HDTV. J Soc Inf Display 2006;14(5):477–85.
[3] Yabushita R, Hata K, Sato H, Saito Y. Development of compact field emission scanning electron microscope equipped with multiwalled carbon nanotube bundle cathode. J Vac Sci Technol B 2007;25(2):640–2.
[4] Dean KA, Chalamala BR. Experimental studies of the cap structure of single-walled carbon nanotubes. J Vac Sci Technol B 2003;21(2):868–71.
[5] Hata K, Takakura A, Saito Y. Field emission from multiwall carbon nanotubes in controlled ambient gases, H_2, CO, N_2 and O_2. Ultramicroscopy 2003;95:107–12.
[6] Liu W, Hou S, Zhang Z, Zhang G, Gu Z, Luo J, et al. Atomically resolved field emission patterns of single-walled carbon nanotubes. Ultramicroscopy 2003;94(3–4):175–82.
[7] Oshima C, Mastuda K, Kona T, Mogami Y, Komaki M, Murata Y, et al. Young's interference of electrons in field emission patterns. Phys Rev Lett 2002;88(3):038301–4.
[8] Buldum A, Lu JP. Electron field emission from carbon nanotubes: modeling and simulations. Mol Simul 2004;30(4):199–203.
[9] Khazaei M, Farajian AA, Kawazoe Y. Field emission patterns from first-principles electronic structures: application to pristine and cesium-doped carbon nanotubes. Phys Rev Lett 2005;95(17):177602–4.
[10] Lee JH, Lee SH, Kim WS, Lee HJ, Heo JN, Jeong TW, et al. Uniformity measurement of electron emission from carbon nanotubes using electron-beam resist. J Vac Sci Technol B 2005;23(2):718–22.
[11] Kumar M, Kakamu K, Okazaki T, Ando Y. Field emission from camphor-pyrolyzed carbon nanotubes. Chem Phys Lett 2004;385(3–4):161–5.
[12] Bonard JM, Croci M, Klinke C, Conus F, Arfaoui I, Stöckli T, et al. Growth of carbon nanotubes characterized by field emission measurements during chemical vapor deposition. Phys Rev B 2003;67(8):085411–2.
[13] Saito Y, Hamaguchi K, Hata K, Uchida K, Tasaka Y, Ikazaki F, et al. Conical beams from open nanotubes. Nature (London) 1997;389:554–5.
[14] Edgcombe CJ, Valdre U. Microscopy and computational modelling to elucidate the enhancement factor for field electron emitters. J Microsc 2001;203:188–94.
[15] Walker DG, Zhang W, Fisher TS. Simulation of field-emitted electron trajectories and transport from carbon nanotubes. J Vac Sci Technol B 2004;22(3):1101–7.
[16] Sanchez JA, Wong BT, Mengüç MP, Albella P. Field emission and electron deposition profiles as a function of carbon nanotube tip geometries. J Appl Phys 2007;101(11):114310–3.
[17] Filip LD, Nicolaescu D, Tanemura M, Kanemaru S, Itoh J. Ring-shaped images as a result of nonuniform field emission from capped carbon nanotubes. J Vac Sci Technol B 2005;23(2):649–56.
[18] Marchand M, Journet C, Adessi C, Purcell ST. Ring patterns in high-current field emission from carbon nanotubes. Phys Rev B 2009;80(24):245425–6.
[19] Fisher TS, Walker DG, Weller RA. Analysis and simulation of anode heating due to electron field emission. IEEE Trans Compon Pack Technol 2003;26(2):317–23.
[20] Zhu W, Bower C, Zhou O, Kochanski G, Jin S. Large current density from carbon nanotube field emitters. Appl Phys Lett 1999;75(6):873–5.
[21] Milne WI, Teo KBK, Amaratunga GAJ, Legagneux P, Gangloff L, Schnell JP, et al. Carbon nanotubes as field emission sources. J Mater Chem 2004;14:933–43.
[22] <http://www.comsol.com>.
[23] Forbes RG. Field-ion imaging old and new. Appl Surf Sci 1996;94–95:1–16.
[24] Wei W, Liu Y, Wei Y, Jiang K, Peng LM, Fan S. Tip cooling effect and failure mechanism of field-emitting carbon nanotubes. Nano Lett 2007;7(1):64–8.